



The Wakefield Induced Emittance Increase Due to the Positron Undulator Module Tapers and Photon Collimators¹

Duncan Scott²



Daresbury Laboratory,
STFC,
Warrington,
Cheshire, WA4 4AD
UK

ABSTRACT

The geometric wakefields of the tapers in the ILC positron undulator line have been calculated using analytic formula and the 2-D code ECHO. The emittance increase due to the wakefields have been calculated for different alignment tolerances of each element. In the worst case scenario considered, where the elements have an alignment tolerance of $\pm 300 \mu\text{m}$ and there are 60 undulator modules and 40 photon collimators, the vertical emittance increase is less than 3%.

¹ Work supported by the Commission of the European Communities under the 6th Framework Programme "Structuring the European Research Area", contract number RIDS-011899.

² d.j.scott@dl.ac.uk

1. Introduction

In the current design for the ILC positron undulator line there are two main elements that have tapers, the photon collimators and the transitions between the room temperature vessels and the cold bore of the undulator module. These tapered sections induce wakefields which can kick an off-axis beam transversely. There is an active research programme in assessing the effects of the Beam Delivery System collimator wakefields and so results from this study can be used to give an estimate of the effects of the undulator line tapers (the tapers can be treated as collimators for this work). There are many references on the subject [1, 2, 3, 4, 5, 6, 7, 8] and the theory is only summarised here. For small displacements off-axis, y , the kick angle, y' , is:

$$y' = K_b y,$$

where K_b is the bunch kick factor. The beam will be off-axis due to jitters in the linac and misalignments of elements. The off-axis displacements and kick angle can be normalised to the rms beam size and divergence, $\sigma_{x,y}$ and $\sigma'_{x,y}$ respectively giving:

$$A = K_b \frac{\sigma_{x,y}}{\sigma'_{x,y}},$$

where A is now a factor characterising the strength of the kick. The combination of kicks can dilute the beam emittance. The emittance dilution, $\frac{\Delta\varepsilon}{\varepsilon}$, for a displacement off-axis of $n\sigma_{x,y}$ is simply [9]:

$$\frac{\Delta\varepsilon}{\varepsilon} = (0.4nA)^2,$$

Using these formula the emittance dilution for a given set of alignment tolerances can be calculated. First the electron beam properties, tapers and kick factors need to be defined.

2. Electron Beam Properties

The assumed beam properties are given in Table 1. The beam emittance values are those at the start of the main linac (i.e. at ~ 5 GeV) [10].

Parameter	Symbol	Unit	Value
Emittance	$\varepsilon_x, \varepsilon_y$	m.rad	$2.9 \cdot 10^{-11}, 8.2 \cdot 10^{-14}$
rms Bunch Length,	σ_z	μm	300
Particles per Bunch	N	10^{10}	2
Beam Energy		GeV	150
Beam Divergence	σ'_x, σ'_y	μrad	1.99, 0.11

Table 1: relevant ILC electron beam properties.

The undulator lattice beta functions are shown in Figure 1 [11] from which the beam-sizes and divergences can be calculated, the beam-sizes are shown in Figure 2, and the divergences in Table 1 (away from the quadrupoles the divergence is constant).

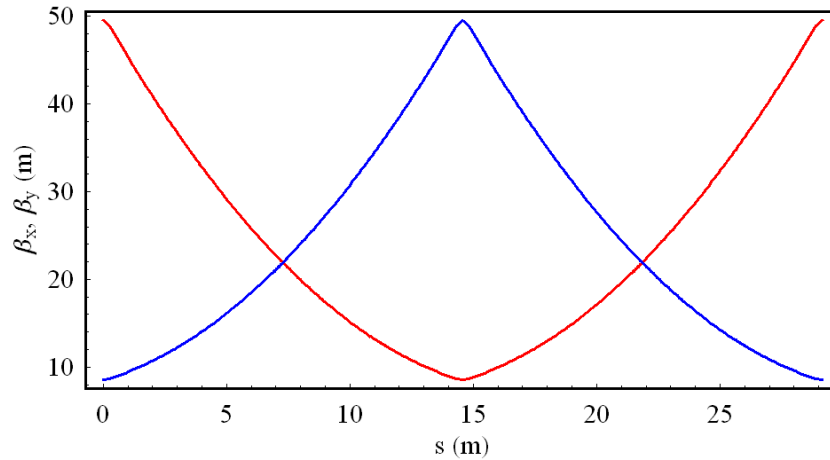


Figure 1: The undulator cell horizontal (red) and vertical (green) beta functions, the quadrupoles are situated at the start, end and in the middle of the cell.

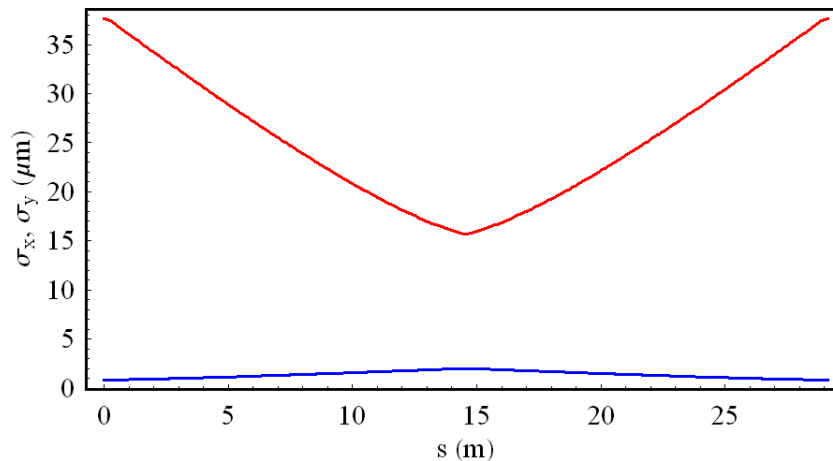


Figure 2: The horizontal (red) and vertical (blue) rms electron beam-size through the undulator cell.

3. Geometry of the Tapered Sections

Photon Collimators

The photon collimators are needed to mask undulator photons that would be incident on the undulator vessel walls and result in vacuum pressure increase via photon stimulated desorption [12]. To have any effect these photon collimators must have an aperture less than the undulator vessel (5.85 mm). As yet there is no engineering design, but an assessment of the effects of likely parameters can be made. Their design is assumed to be an axially symmetric taper down to a minimum aperture and then a similar taper back up to the nominal vessel radius of 18 mm. There is no flat portion between the two tapers. Figure 3 and Table 2 give the length of the collimator as a function of the collimator angle for a 0.5 mm and 2.5 mm radius

aperture, and. There is little difference in collimator length between the two apertures. To keep the length of the collimator reasonably short a 0.1 rad 2 mm radius aperture was used.

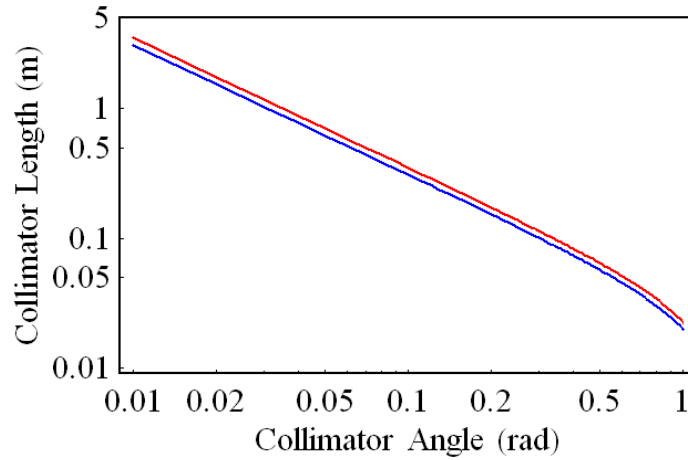


Figure 3: Total length of collimator as a function of collimator angle for a 0.5 mm radius aperture (red) and a 2.5 mm radius aperture (blue).

Parameter	Unit	Value					
		0.05	0.1	0.2	0.3	0.5	1
Angle	rad	0.05	0.1	0.2	0.3	0.5	1
0.5 mm radius aperture	m	0.70	0.35	0.17	0.11	0.06	0.022
2 mm radius aperture	m	0.62	0.31	0.15	0.10	0.057	0.020

Table 2: Collimator lengths for different taper angles and aperture radius.

Undulator Transitions

The undulator line consists of a FODO cell lattice with three undulator modules between the quadrupoles. The vessels for the quadrupoles are at room temperature and require traditional pumping solutions with a relatively large bore vessel. The transitions from the large diameter room temperature vessel to the small diameter cold-bore undulator vessel are tapered sections at the start and end of each undulator module. Currently there are two designs for the tapered section.

Shielded Bellows Layout

Figure 4 shows the shielded bellows layout [13]. The dimensions for the tapers are given in **Table 3**, where the flat length is the distance to the next taper. The system is axially symmetric about the centre.

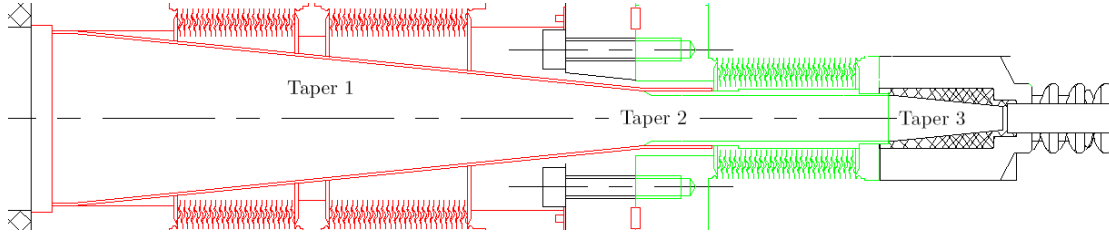


Figure 4: Layout of the shielded bellows design for the tapered section of the undulator. The large bore room temperature vessel is on the left and the small cold-bore undulator vessel to the right. Taper 1 can be seen on the left in red, taper 2 is the green chamfer by the sliding joint with the red taper and taper 3 is where the green vessel enters the undulator magnet on the right.

Taper	Large Diameter (mm)	Small Diameter (mm)	Flat Length (mm)	Taper Angle (mrad)
Taper 1	36	11.7	0	100
Taper 2	11.7	10	39	524
Taper 3	10	5.85	3700	100

Table 3: Taper dimensions for the shielded bellows layout one.

Vacuum Problems with the Shielded Bellows Layout

The shielded bellows design leads to trapped air volumes between the bellows and the shields. In order to effectively pump these volumes holes would need to be made in the tapered shield. This technique is used to pump gas trapped behind the beam screen in the LHC dipole magnets [14], however, calculating the wakefield effects of such holes for the ILC is not trivial [15, 16]. The theory from the LHC studies can be used if the following conditions are met [17]:

$$s \ll R, \quad \frac{\omega s}{c} \ll 1, \quad \text{and} \quad g \ll s,$$

where s is the dimension of the hole, R is the radius of the vessel, g the thickness of the liner c the speed of light and ω the frequency of the applied field. Typical values for single bunch effects at the LHC are given in Table 4.

s	R	$\omega s c^{-1}$
mm	mm	
1.5	24	0.022
8	24	0.12

Table 4: LHC values for the parameters relevant for the wakefield effects of slotted pumping holes.

Therefore to be able to use the same theory as the LHC, and give similar ratios as in Table 4, the ILC would require the dimension of the hole to be ~ 3 microns by ~ 17 microns, (by condition 2). However, by using holes of this dimension it would

then violate condition 3. This means that either a different theory,³ or a different layout of the undulator tapered sections must be used.

Unshielded Bellows Layout

A schematic of a second layout with unshielded bellows is shown in Figure 5. To allow for pumping there is gap between the red bellows and the blue taper. At the corner closest to the red bellows the taper has a 2 mm radius and is 3.81 mm away from the end of the bellows longitudinally. The dimensions for the tapers are given in **Table 5**, where the flat length is the distance to the next taper. The system is axially symmetric about the centre.

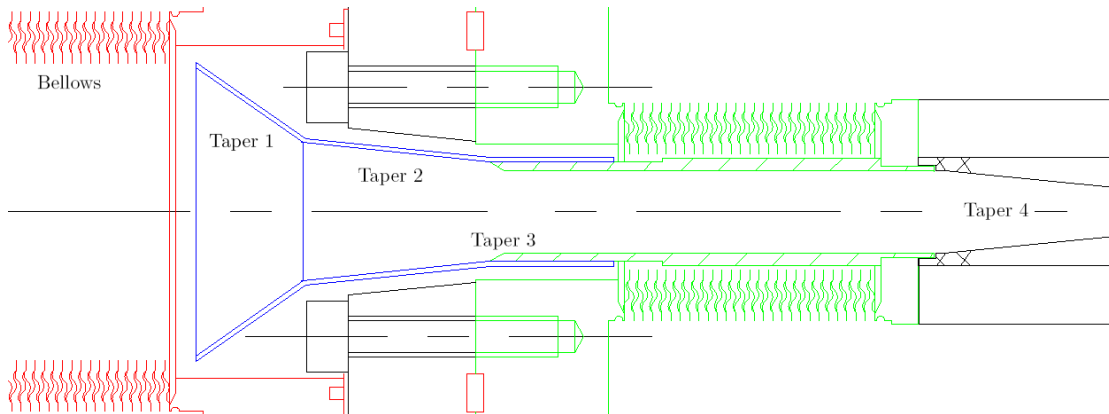


Figure 5: Layout of the unshielded bellows design for the tapered section of the undulator. The large bore room temperature vessel is on the left, with the exposed red bellows, and the small cold-bore undulator vessel to the right. Taper 1 and taper 2 can be seen on the left in blue, taper 3 is the green chamfer by the sliding joint with the blue taper and taper 4 is where the green vessel enters the undulator magnet on the right.

The dimensions for the tapers are given in Table 5, where the flat length is the distance to the next taper. The system is axially symmetric about the centre. There are 23 corrugations of the bellows with a pitch of 1.4 mm and a inner radius of 17.65 mm and an outer radius of 24 mm.

Taper	Large Diameter (mm)	Small Diameter (mm)	Flat Length (mm)	Taper Angle (mrad)
Taper 1	37.65	17	0	611
Taper 2	17	11.7	0	100
Taper 3	11.7	10	39	524
Taper 4	10	5.85	3700	100

Table 5: Taper dimensions for the unshielded bellows layout.

³ N.B. this doesn't mean that if the three conditions were met things would be ok, it just means that the LHC theory could be used to calculate the effect.

4. Kick Factors

The bunch kick factor, K_b , is given by [4]:

$$K_b = 4\pi\epsilon_0 \frac{Nr_e}{\gamma} k_{\perp},$$

where ϵ_0 the permittivity of free space, r_e is the classical electron radius, γ is the relativist factor for the bunch, N the number of particles in the bunch and k_{\perp} is the wakefield kick factor. Generally there is a part for each multipole component of the beam, however only the dipole order transverse kick factor has been considered. The wakefield kick factors, k_{\perp} , from the different elements have been calculated using the numerical code ECHO [18], and cross checked using analytic expressions where appropriate.

Photon Collimator Wakefield Kick Factors

The analytic expression for the inductive wakefield kick of a Gaussian bunch (of rms length σ_z) passing through an axially symmetric round collimator of large radius b_1 , small radius b_2 and taper angle θ is [3]:

$$k_{\perp} = \frac{Z_0 c}{2\pi^{3/2} b_1^2} \frac{\theta b_1}{\sigma_z} \left(1 - \frac{b_1}{b_2}\right),$$

where Z_0 is the impedance of free space and c is the speed of light. This expression is compared to the transverse loss factor as calculated in ECHO for different θ , b_2 and a b_1 of 18 mm in Figure 6. There is a good agreement between the two methods.

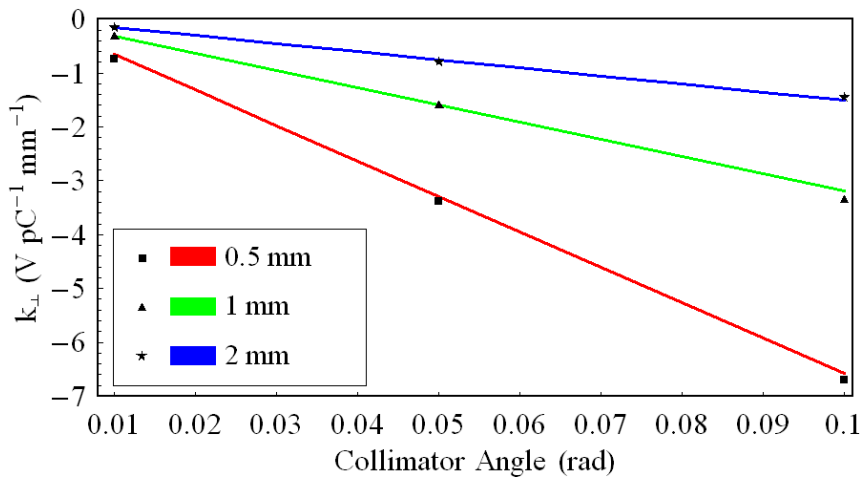


Figure 6: k_{\perp} calculated using the analytic expression for a short round collimator (lines) and ECHO (points) for different taper angles, θ , and small collimator aperture, b_2 .

Undulator Wakefield Kick Factors

The undulator tapers are in the diffractive regime. Again there are analytic formula for axially symmetric round tapers. Interestingly the wakefield kick factors are independent of bunch length. For a short collimator (i.e. the length of the flat part is approaching zero the wakefield kick factor is [1]:

$$k_{\perp} = \frac{Z_0 c}{2\pi} \left(\frac{1}{b_1^2} - \frac{b_1^2}{b_2^4} \right).$$

Table 6 shows the comparison between the analytic expression and ECHO for the shielded bellows layout. Also shown is the ECHO result for the unshielded layout. The bellows do not contribute much to the wakefield kick, just $0.01 \text{ V pC}^{-1} \text{ mm}^{-1}$ as calculated in ECHO for 23 corrugations of the bellows.

Model	Unit	k_{\perp}
Analytic, Shielded Layout	$\text{V pC}^{-1} \text{ mm}^{-1}$	1.34
ECHO, Shielded Layout	$\text{V pC}^{-1} \text{ mm}^{-1}$	0.93
ECHO, Unshielded Layout	$\text{V pC}^{-1} \text{ mm}^{-1}$	0.96

Table 6: analytic and ECHO values of k_{\perp} for the different undulator layouts.

Bunch Kick Factors

The bunch kick factors for the different elements are shown in Table 7.

Element	K_b
Collimator	$3.19 \cdot 10^{-5}$
Shielded Undulator	$1.97 \cdot 10^{-5}$
Unshielded Undulator	$2.03 \cdot 10^{-5}$

Table 7: K_B for each element in the undulator line.

6. Emittance Increases

The emittance increases for the undulator line can now be calculated. An example cell layout is shown in Figure 7, where there are two undulators per module. This is just representative, for example further work may decrease the number of photon collimators that are required. Using this layout and Figure 2 the ratios, $\frac{\sigma_{x,y}}{\sigma'_{x,y}}$, can be calculated. The amplification factors for each element in the cell (in the horizontal and vertical planes) are shown in Figure 8 for the unshielded bellows case (the worst).

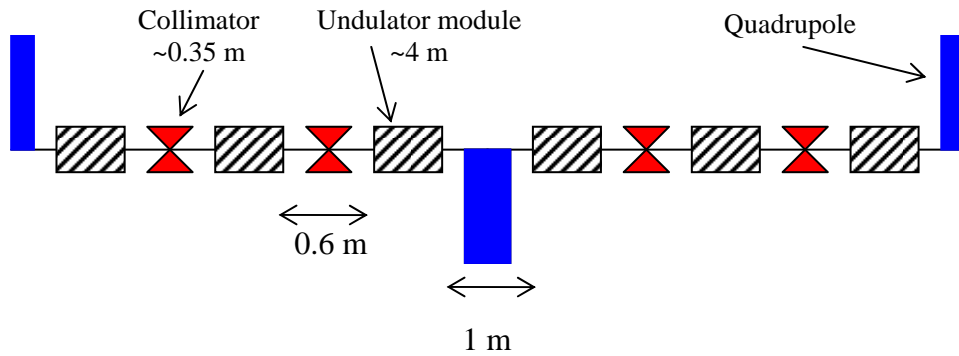


Figure 7: layout of undulator cell used for the emittance increase study.

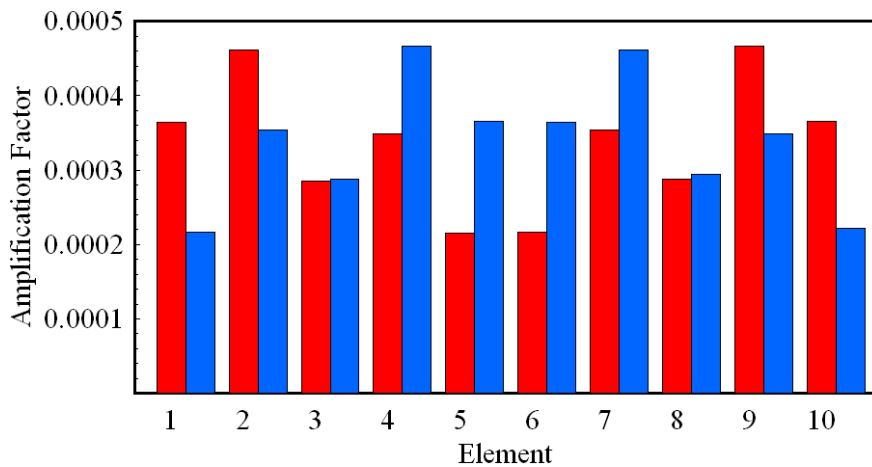


Figure 8: amplification factors of each element from each undulator and collimator (in order from Figure 7) through the undulator cell in the x (red) and y (blue) planes.

Emittance Increase for a perfectly aligned undulator line

For perfectly aligned elements the only contribution to an emittance dilution is from the beam jitter. Using the conservative estimate of 0.5 in both planes as the transverse displacement jitter of the beam the emittance is increased by a factor of $4.8 \cdot 10^{-7}$ over 10 cells.

Emittance Increase for a misaligned undulator line

In reality each element will be misaligned from the axis. This misalignment has been incorporated into the expression for the emittance increase to give an estimate of the required alignment tolerances for the undulator line. A line consisting of 10 cells similar to Figure 7 was created and each element randomly misaligned by an amount following a Gaussian distribution. Different rms values for the Gaussian distribution were considered, however the misalignments were truncated at 300 microns as it is assumed that the elements can be aligned to that accuracy by the survey team. The line was simulated 10 000 times for each different rms value. An example of the distribution of vertical emittance increases for a standard deviation of 100 microns is shown in Figure 9. The mean vertical and horizontal emittance increase for each rms displacement over the 10 000 iterations is shown in Figure 10.

The mean increase is only 2.7% in the vertical plane for a 300 microns rms displacement of each element.

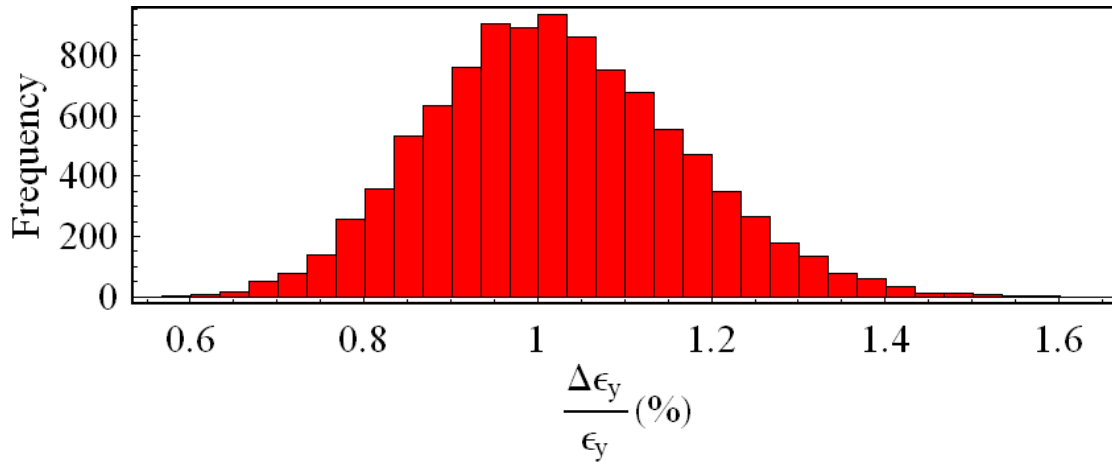


Figure 9: increase in ε_x for 10 000 iterations with each element randomly displaced following a Gaussian distribution with an rms of 100 μm , truncated at 300 μm .

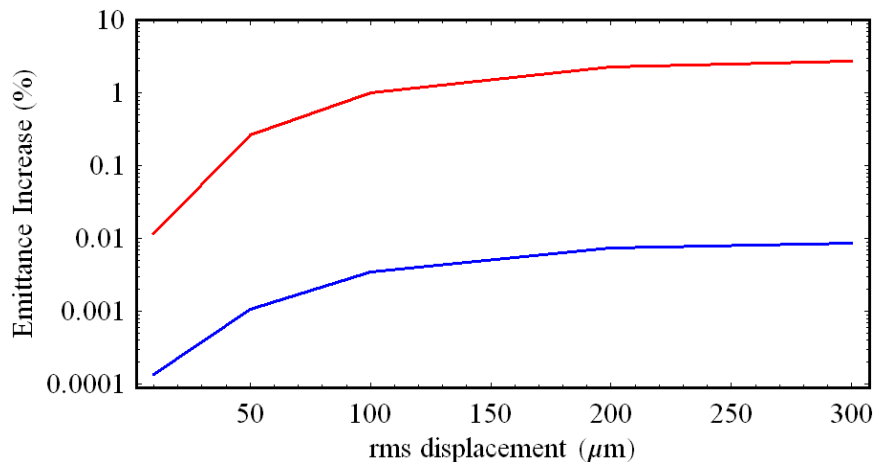


Figure 10: Mean percentage increase in emittance in the vertical (red) and horizontal (blue) planes from for increasing rms displacement of each element in the undulator line.

5. Conclusions

The emittance increases due to the wakefield kicks of tapered elements in the undulator line have been shown to be small. If elements can be aligned with an rms value of 300 μm the emittance increase is less than 3% in the vertical plane. As yet there is no tolerance for the allowable emittance increase, however a maximum of 3% seems acceptable. This increase is for an line consisting of 60 undulator modules and 40 collimators, which is the maximum envisaged number of elements, further work could reduce the number of elements to 50 undulator modules and 20 collimators.

The code ECHO has been used and it would be worthwhile to check the results using another code.

For the unshielded bellows design there is not a continuous conducting path for the image currents to follow. Therefore some modifications of taper 1 to make sure it is in electrical contact with the bellows need to be made. If done correctly these should not affect the geometric wakes.

The assumed theory is only true for small deviations off-axis. A full simulation including higher order terms [19] could be carried out if necessary. It may be that the large displacements off-axis considered, up to 0.4 mm, require the inclusion of higher order terms.

6. References

- 1 P. Tenenbaum “*Collimator Wakefield Calculations for the ILC-TRC Report,*” LCC-Note-0101, August 2002.
- 2 NLC Post-Linac Collimation Task Force, “*New Post-Linac Collimation System for the Next Linear Collider,* SLAC, LCC-Note LCC-0052, 2001
- 3 P. Tenenbaum, “Direct measurement of the transverse wakefields of tapered collimators,” PR-STAB 10, 034401 (2207).
- 4 C.D. Beard and R.M. Jones, “Numerical Simulations of Collimator insertions using MAFIA”, EUROTeV-Report-2006-103
- 5 G.V. Stupakov, “High-Frequency Impedance of Small-Angle Collimators, PAC2001
- 6 I. Zagorodnov, T. Weiland, K. Bane, “Calculation of Collimator Wakefields, PAC 2003
- 7 I. Zagorodnov, K.F. Bane “Wakefield Calculations for FD Collimators” EuroTeV-Report-2006-074
- 8 Nk. Watson et al. “Direct Measurement of Geometric and Resistive Wakefields in Tapered Collimators for the International Linear Collider” EPAC 2006
- 9 NLC Post-Linac Collimation Task Force, “*New Post-Linac Collimation System for the Next Linear Collider,* SLAC, LCC-Note LCC-0052, 2001
- 10 International Linear Collider Reference Design Report, Draft Version, Feb 2007
- 11 Courtesy of J. Jones, DL, CCLRC.
- 12 O.B. Malyshev and D.J. Scott, “*Vacuum Systems for the ILC helical undulator*” EUROTeV-Report-2006-086
- 13 S. Carr, RAL, STFC
- 14 A. Chao, “Summary of the Working Group on Impedances” Particle Accelerators, V50, Page 1-17, (1995)

-
- 15 S.S. Kurennoy, "Impedance Issues for the LHC Beam Screen", Particle Accelerators, V50 page 167-175, (1995)
- 16 G.V. Stupakov, "Coupling Impedance of a long slot and an array of slots in a circular vacuum chamber," Phy.Rev. E V51, No.4 April 1995, Page 3515-3521
- 17 A.V. Fedotov, "Longitudinal Coupling Impedance of a Hole in an Accelerator Beam Pipe at Finite Frequencies". PhD Thesis, University of Maryland, 1997
- 18 I. Zagorodnov & T. Weiland "TE/TM field solver for particle beam simulations without numerical Cherenkov radiation, PR-STAB, 8, 042001 (2005)
- 19 A. Bungau and R.Barlow, "*Large Simulation of High Order Short Range Wakefields*," EPAC 2006.